Heliyon 10 (2024) e39939

Contents lists available at ScienceDirect

Heliyon

journal homepage: www.cell.com/heliyon

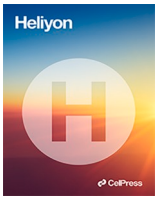

Research article

# Protective effects of Shexiang-Tongxin dropping pill against acute myocardial infarction in rats through inhibition of apoptosis and ERK/MAPK signaling pathways

Jun Yan [a,b,1], Hanbing Liu [a,b,1], Jiaxin Shang [b], Qianqian Fang [d], Jianfeng Ye [d], Xiaoyan Lu [b,c,e,*], Xiaohui Fan [a,b,c,e,**]

[a] State Key Laboratory of Chinese Medicine Modernization, Tianjin University of Traditional Chinese Medicine, Tianjin, 301617, China
[b] Pharmaceutical Informatics Institute, College of Pharmaceutical Sciences, Zhejiang University, Hangzhou, 310058, China
[c] State Key Laboratory of Chinese Medicine Modernization, Innovation Center of Yangtze River Delta, Zhejiang University, 314100, Jiaxing, China
[d] Inner Mongolia Conba Pharmaceutical Co., Ltd., Ordos, 017000, China
[e] Jinhua Institute of Zhejiang University, Jinhua, 321299, China

ARTICLE INFO

*Keywords:*
Shexiang-tongxin dropping pill
Acute myocardial infarction
Network pharmacology
ERK/MAPK signaling pathway
Apoptosis signaling pathway

ABSTRACT

Acute myocardial infarction (AMI) remains a significant health challenge globally, highlighting the ongoing need for effective treatments. Shexiang-Tongxin dropping pill (STDP) is widely utilized as a therapeutic option for AMI in China and Southeast Asia. However, the intricate mechanisms of action of STDP against AMI remain largely unknown. The pharmacodynamic effects of STDP in treating AMI were evaluated both *in vitro* and *in vivo* using human umbilical vein endothelial cell oxygen-glucose deprivation, RAW264.7 cell inflammatory injury, and rat left anterior descending surgery models. The whole transcriptome sequencing was performed to analyze gene expression changes in experimental rat hearts after left anterior descending surgery. An integrative approach combining network pharmacology and sequencing data was used to determine the multi-target and multi-pathway mechanisms underlying the action of STDP against AMI. Molecular docking was conducted to identify the primary anti-AMI ingredients in STDP. STDP treatment significantly resisted AMI *in vivo* and protected against inflammatory and hypoxic injuries *in vitro*. It resulted in 63 % (901 of 1430) of genes showing restorative regulation in the AMI disease network, relating to the TGF-β, PI3K, apoptosis, and MAPK pathways. Validation experiments indicated that inhibiting apoptosis and ERK/MAPK pathways by reducing Bax and p-ERK1/2 expression levels in rat hearts may be a crucial mechanism of STDP against AMI. Molecular target prediction indicated that tanshinone IIA, salvianolic acid A, salvianolic acid B, and resibufogenin were the essential pharmacodynamic substances of STDP in AMI treatment. This study sheds light on novel mechanisms by which STDP rebalances the AMI disease network through its multi-target and multi-pathway effects. The findings offer data support for the more precise clinical application of STDP.

* Corresponding author. Pharmaceutical Informatics Institute, College of Pharmaceutical Sciences, Zhejiang University, #866 Yuhangtang Road, Hangzhou, 310058, China.
** Corresponding author. Pharmaceutical Informatics Institute, College of Pharmaceutical Sciences, Zhejiang University, #866 Yuhangtang Road, Hangzhou, 310058, China.
*E-mail addresses:* luxy@zju.edu.cn (X. Lu), fanxh@zju.edu.cn (X. Fan).
[1] These authors contributed equally to this article.

https://doi.org/10.1016/j.heliyon.2024.e39939
Received 6 March 2024; Received in revised form 27 October 2024; Accepted 28 October 2024
Available online 29 October 2024

## 1. Introduction

Acute myocardial infarction (AMI) continues to be a leading contributor to worldwide health challenges, with more than 7 million newly affected individuals [1] and an annual mortality of 17.3 million cases [2]. The inflammatory response to ischemic syndrome is crucial in defining the myocardial infarction (MI) size and consequent negative remodeling of the left ventricular [3]. Despite the significant improvements in managing AMI over the past 30 years, the 30-day mortality rate remains at 7.9 %, and the 1-year mortality rate is approximately 10 % [4,5], threatening the developing and developed countries with high economic burden. AMI therapies require improvements because the currently available strategies have many limitations. The most effective treatment for AMI is primary percutaneous coronary intervention (PPCI); however, this strategy has disadvantages, such as limited time of door-to-balloon, critical complications, and high healthcare costs. Other drug treatments, such as antiplatelet agents, β-blockers, and angiotensin-converting enzyme inhibitors, are directed at a single pathway or target and induce severe adverse reactions, such as cardiogenic shock and bleeding complications [1,6,7]. Several therapies targeting the inflammatory response after AMI, such as the subcutaneous injection of IL-1 receptor antagonists and intravenous injections of Tocilizumab and rhuMAb CD18, have also received attention recently. Notably, some of these therapies, which focus on a single inflammatory target, showed no benefits in reducing MI size or improving clinical prognosis [3,8–10]. Thus, developing a multi-target approach with limited adverse reactions may be a direction for AMI treatment.

Shexiang-Tongxin dropping pill (STDP), sanctioned by the China National Medical Products Administration, is a common nationally protected Traditional Chinese Medicine (TCM) product in the treatment of cardiovascular diseases within China and Southeast Asia [11,12]. Clinical evidence showed that STDP benefits the improvement of left ventricular function, coronary slow flow phenomenon, and inflammation in patients with AMI, followed by PPCI [13,14]. Similarly, pre-clinical studies demonstrated that STDP alone can ameliorate coronary microcirculation disturbance and cardiac dysfunction after myocardial ischemia-reperfusion in pigs [15] and protect against isoproterenol (ISO)- or pituitrin-induced myocardial ischemia injury in rats [16,17]. These studies suggest that STDP is an effective drug for treating AMI with highly acceptable safety. However, the multi-target mechanisms of STDP against AMI at the system level are poorly understood.

Network pharmacology approaches are used for unbiased elucidation of mechanisms of action of drugs and are particularly suitable for revealing the multi-target effects of TCM [18]. The complex interactions between TCM and diseases can be revealed by this approach [19]. Moreover, it enables the effective mapping of critical nodes implicated in disease at the system level and the identification of the multi-target activity of TCM on this disease network [20]. Our team and many other researchers have successfully elucidated the mechanisms of TCM through network pharmacology [21–25]. For example, the cardiovascular protective effects of the Yangxinshi table are primarily related to the coagulation cascades, neurotrophins, and AMPK signaling pathways, as revealed by a network pharmacology strategy [21]. By combining compound-target-pathway network analysis with both *in vivo* and *in vitro* studies, a multi-component, multi-target, and multi-pathway mode of action of QiShenYiQi against MI was clarified in our previous study [22]. Network pharmacology and RNA sequencing revealed that the inhibition of mitochondrial homeostasis-mediated apoptosis through the stabilization of β-tubulin and stimulation of SIRT1 protected sinoatrial node cells in cardiac hypoxic environments [23].

In this study, whole transcriptome sequencing was performed on experimental rat hearts to explore the regulatory effects of STDP on AMI rats at the genetic level. Network pharmacology technique was further used to comprehensively identify the complex multi-target and multi-pathway mechanisms of action of STDP for AMI treatment. Moreover, *in vivo* validation experiments and molecular docking studies were performed to validate the precision of the vital targets and forecast the essential anti-AMI ingredients in STDP.

## 2. Materials and Methods

### 2.1. Drug

STDP (Lot No. 170204) was supplied by Inner Mongolia Conba Pharmaceutical Co., Ltd. (Ordos, China; National Medical Products Administration Med Drug Permit No. Z20080018). The seven medicinal ingredients in STDP are *Salvia miltiorrhiza* Bunge, *Panax ginseng* C.A.Mey., *Borneolum Syntheticum*, *Moschus* (the dried secretion of musk sac of adult male *Moschus berezovskii* Flerov, Moschus *sifanicus* Przewalski, or *Moschus moschiferus* Linnaeus), *Bufonis Venenum* (the dried secretion of *Bufo bufo gargarizans* Cantor, or *Bufo melanostictus* Schneider), *Bovis Calculus Artifactus* (processed with cow bile powder, hyodeoxycholic acid, cholic acid, taurine, bilirubin, cholesterol, and trace elements, among others), and *Fel Ursi* (the dried bile in the gallbladder of *Ursus arctos* Linnaeus, or *Selenarctos thibetanus* G. Cuvier). The production process and chemical fingerprint of STDP were extensively described in our previous study [26]. Seven medicinal herbs were processed into STDP following the method outlined in the Chinese Pharmacopoeia (2020 Edition).

### 2.2. Animal experiments

Male Sprague-Dawley rats weighing between 200 and 220 g, obtained from Shanghai SLAC Laboratory Animal Co., Ltd., were accommodated in a regulated environment (25 ± 1 °C, 12-h light/dark cycles) with free access to food and water. Animal experiments adhered to the guidelines of the Animal Care and Use Committee of Zhejiang University School of Medicine. The specific STDP dose administered to rats was calculated based on a human equivalent dosage of 210 mg/60 kg and the body surface area conversion value of 6.2 for rats and humans [27]. The calculated clinically equivalent STDP dose in rats was approximately 22 mg/kg/day, and a twice clinically equivalent STDP dose was approximately 43 mg/kg/day. Based on the preliminary study (Supplementary Fig. 1), we found

that the twice clinically equivalent STDP dose had a more significant therapeutic effect on AMI than the clinically equivalent STDP dose did. Therefore, the twice clinically equivalent STDP dose was used for the subsequent experiments. After acclimatization, rats were randomly divided into three groups, namely Sham, Model, and STDP. The STDP group was administered intragastrically with 43 mg/kg STDP daily in a volume of 1 mL/100 g of body weight. The Sham and Model groups were administered 1 % sodium carboxymethyl cellulose at 1 mL/100 g body weight. The drug was administered once daily for 7 days. Following this, the AMI model was established through left anterior descending (LAD) coronary artery ligation surgery [28,29], with the Sham group undergoing pericardial laceration without ligation. Drug administration continued for 3 days after surgery.

### 2.3. Echocardiography

Following the completion of the trial, the rats were anesthetized using 1.5 % pentobarbital sodium. The thoracic fur was meticulously removed, and the rats were securely positioned on the operating platform. Vital cardiac functional parameters and transthoracic echocardiographic images were acquired using the VINNO D6 VET ultrasound system (equipped with a probe, Vinno Technology Ltd., Suzhou, China) [30,31].

### 2.4. Enzyme-linked immunosorbent assay (ELISA)

The concentrations of inflammatory cytokines interleukin (IL)-6 and IL-1β in rat serum were quantified using the Rat IL-6 ELISA Kit and the Rat IL-1β ELISA Kit from Elabscience Biotechnology Ltd., Wuhan, China, respectively. The measurements were performed in strict accordance with the protocols provided by the manufacturer.

### 2.5. Estimation of myocardial infarct size

The blood residue in the heart removed in the previous step was rinsed off with saline, and four hearts from each group were frozen at −20 °C for around 2 h. The frozen hearts were sliced horizontally into five uniform slices, approximately 2 mm thickness each. The heart slices were stained with 1 % 2,3,5-triphenyl tetrazolium chloride (TTC, Solarbio Co., Ltd., Beijing, China, G3005) maintained at 37 °C for a quarter of an hour in a water bath, and were subsequently fixed with 4 % paraformaldehyde. Photographs were taken the next day, and the infarct area was analyzed using the ImageJ software v1.53a to calculate the relative infarct size of each rat heart. The formula was as follows:

$$\textit{Infarct percent size} = \frac{\textit{Sum of infarct area of each heart section}}{\textit{Sum of the total area of each heart section}} \times 100\% \quad (1)$$

### 2.6. Histopathological evaluation

Three rat hearts from each group were fixed in 4 % paraformaldehyde for 48 h, embedded in paraffin, and cut into 4 μm sections for hematoxylin-eosin (HE) and terminal deoxynucleotidyl transferase-mediated dNTP nick end labeling (TUNEL) staining. HE staining was used to observe histopathological changes in heart tissue, and TUNEL staining was used to investigate cardiac tissue apoptosis. Images were taken with a Nikon inverted fluorescence microscope (Nikon Eclipse Ti-SR, Tokyo, Japan).

### 2.7. Cell culture

Human umbilical vein endothelial cells (HUVECs) and RAW264.7 murine macrophage cells were purchased from the Chinese Academy of Sciences Typical Culture Collection Committee Cell Bank (Shanghai, China). Cells were cultured in a high-glucose Dulbecco's modified Eagle's medium (DMEM, Gibco, ThermoFisher Scientific Inc., Waltham, MA, USA) supplemented with 100 U/mL penicillin, 100 μg/mL streptomycin (Gibco, ThermoFisher Scientific), and 10 % heat-inactivated fetal bovine serum (Gibco, ThermoFisher Scientific). The cell culture incubation conditions were set to 37 °C and 5 % $CO_2$.

### 2.8. Nitric oxide assay

RAW264.7 cells were cultured normally in 96-well plates for 24 h. Subsequently, 200 ng/mL lipopolysaccharide (LPS), either alone or in combination with varying concentrations of STDP (25, 50, 100, and 200 μg/mL) or 1.276 μM dexamethasone (positive drug), was incubated for an additional 24 h. Nitric oxide levels in the cell supernatants were subsequently determined using a nitric oxide assay kit (Shanghai Beyotime Biotechnology Co., Ltd, S0021M).

### 2.9. Cell counting kit-8 (CCK-8) assay

The oxygen-glucose deprivation (OGD) model was used to evaluate the anti-endothelial hypoxic injury effect of STDP. HUVECs were seeded in 96-well flat-bottom plates at a density of $8 \times 10^4$ cells per well. Following a 24-h incubation under standard conditions, the original culture medium was discarded, and the cells were then divided into three groups, namely Control, Model, and STDP treatment. Cells in the Control group were supplemented with a high-glucose DMEM complete medium, those in the OGD Model group

were supplemented with a DMEM sugar-free medium, and those in the STDP treatment group were supplemented with 25 μg/mL of STDP (DMEM sugar-free medium diluted). The cells in all groups were incubated under hypoxic conditions (95 % nitrogen, 5 % carbon dioxide) for 6 h. Subsequently, the original culture medium was substituted with 10 % CCK-8 solution, and the cells were incubated for an additional 2 h in the dark. The absorbance readings of the solutions were taken at 450 nm using the Infinite M1000 Pro spectrophotometer (TECAN Ltd., Männedorf, Germany).

### 2.10. Transcriptome sequencing and data analysis

Total RNA was extracted from the heart tissue of three rats in each group using Trizol™ reagent (Thermo Fisher Scientific, MA, USA). The RNA integrity was verified through agarose gel electrophoresis. Subsequently, an Illumina NEBNext® Ultra™ RNA Library Prep Kit (NEB, MA, USA) was used to build sequencing libraries following the provided protocols. A Qubit 2.0 Fluorometer (Thermo Fisher Scientific, MA, USA) was used to determine the DNA content, and an Agilent 2100 Bioanalyzer (Agilent, CA, USA) was used to evaluate the integrity of library DNA. Only the DNA samples that passed the quality inspection were selected for sequencing on the Illumina HiSeq X platform (Illumina, CA, USA).

The sequenced image data were converted to sequence reads data using CASAVA (Illumina, CA, USA) base identification. The sequence reads data were referenced and compared using HISAT2 v2.0.5, followed by new gene prediction with StringTie. The featureCounts tool in subread software was applied to quantify the gene expression levels and summed to acquire the gene expression matrix of all samples. Differences in quantitative sequencing were analyzed using the DEGseq2 R package v1.16.1 to compare the variations in gene transcript levels among the Sham, Model, and STDP groups and calculate the *P* values and Fold Change. Differentially expressed genes (DEGs) between the Model and Sham groups, as well as the STDP and Model groups, were screened based on *P* values less than 0.05 and an absolute Fold Change greater than 1.5.

### 2.11. AMI disease network construction and analysis

The Dplyr tool in R software was used to extract the rat cardiovascular disease-related genes from the CHD@ZJU3.0 cardiovascular disease database (http://tcm.zju.edu.cn/chd/). These genes were integrated with transcriptome sequencing data to obtain an intersection, and the genes in this intersection were used to construct the AMI disease network based on the protein-protein interactions of these genes analyzed using the String database (https://string-db.org/). The disease network was visualized using Cytoscape V3.8.0 software. Pathway enrichment analysis was performed through the Kyoto Encyclopedia of Genes and Genomes database (https://www.kegg.jp/) to identify the pathways closely related to the onset and progression of the disease.

Based on the constructed AMI disease network, the significant nodes in the network were identified according to the network topology and transcriptomics-based approach (NTRA) previously proposed by our group [20]. Briefly, the NTRA rank was calculated by combining the topological and transcriptomics ranks. The former is a combination of the relative ranking of betweenness and degree, and the latter is a combination of the relative ranking of Fold Change and *P* value ranks. Larger Fold Change indicates greater changes in gene expression, while smaller *P* values represent more significant changes in gene expression. A higher NTRA rank means greater importance of a gene in the disease network.

Upon this basis, we further used the efficiency of recovery regulation (EoR) theory to comprehensively assess the rebalancing effect of STDP on the AMI disease network [32]. We aimed to calculate the gene regulation level (RL) in response to STDP treatment and determine the efficacy of STDP intervention in restoring the genes disrupted by LAD surgery. The calculation was performed according to Eqs. (2) and (3). EoR >0 represented a restorative regulatory effect of STDP treatment on this gene in the AMI disease network.

$$\boldsymbol{RL} = \frac{\boldsymbol{Fold\ Change(STDP/Model)}}{\boldsymbol{Fold\ Change(Sham/Model)}} \tag{2}$$

$$\boldsymbol{EoR} = \mathbf{100\%} - |\mathbf{100\%} - \boldsymbol{RL}| \tag{3}$$

### 2.12. Pathway enrichment analysis

Only genes in the top 50 % of the NTRA rank and with EoR >0 were considered for pathway enrichment analysis. Ingenuity Pathways Analysis (IPA) software and Metascape (https://metascape.org/gp/index.html) were used for pathway enrichment and biological function analyses.

### 2.13. Quantitative real-time PCR (qRT-PCR)

The accuracy of the sequencing data was verified using qRT-PCR. Total RNA was extracted with Trizol reagent (Beyotime Biotechnology, Shanghai, China, R0016), and equal amounts of RNA from each of the three individual samples within a group were mixed to obtain a representative sample for that group. The RNA samples were then reverse transcribed using the QuantiNova Reverse Transcription Kit (QIAGEN, Hilden, Germany), adhering to the protocol provided by the manufacturer. Subsequently, real-time PCR reactions were performed with specific primers with Hieff UNICON® qPCR SYBR Green Master Mix (Yeasen Biotechnology, Shanghai, China, 11198ES03). The primer sequences are presented in Supplementary Table S1. The internal reference gene was *Actb*, and gene expression levels were quantified using the $2^{-\Delta\Delta Ct}$ method. The experiment was performed in triplicates.

### 2.14. Western blot analysis

Heart tissue lysates were generated with radioimmunoprecipitation assay buffer (RIPA, Beyotime Biotechnology, Shanghai, China, P0013B) containing 1 % phenylmethanesulfonyl fluoride (PMSF, Beyotime Biotechnology, Shanghai, China, ST506), and a bicinchoninic acid (BCA) protein assay kit (Thermo Fisher Scientific, MA, USA) was used to measure the concentrations of the protein samples. The same amount of protein samples from three identical samples within a group were mixed and used as a representative sample for that group. The protein samples from each group were transferred to polyvinylidene fluoride (PVDF, Millipore, MA, USA, IPVH00010) membranes through 10 % sodium dodecyl sulfate-polyacrylamide gel electrophoresis (Bio-Rad Laboratories, CA, USA). These PVDF membranes were then blocked using a 5 % skim milk powder solution and incubated overnight at 4 °C with primary antibodies against GADPH (Beyotime Biotechnology, Shanghai, China, AF1186), Bax (Beyotime Biotechnology, Shanghai, China, AF1270), ERK1/2 (Cell Signaling Technology, MA, USA, 9102S), and p-ERK1/2 (Cell Signaling Technology, MA, USA, 8544S). The membranes were then washed four times and incubated with horseradish peroxidase-conjugated secondary antibody for 1 h at room temperature. Finally, the blots were assessed using the Bio-Rad ChemiDocTM imaging system (Bio-Rad Laboratories, CA, USA). To detect the ERK1/2 protein, the PVDF membrane of p-ERK1/2 protein was washed with stripping buffer for 15 min to remove previous signals and re-blocked. Subsequently, the PVDF membrane was incubated at 4 °C overnight with the ERK primary antibody, followed by re-incubation with a secondary antibody and color development. GAPDH served as an internal standard, and the resulting data were processed using Image Lab 6.0 software.

### 2.15. Molecular docking

Canonical SMILES of the 13 key ingredients (taurine, taurodeoxycholic acid, gentisic acid, cinobufotalin, bufalin, cinobufagin, resibufogenin, protocatechualdehyde, danshensu, tanshinone IIA, salvianolic acid A, salvianolic acid B, and salvianolic acid D) of STDP [26] were collected in the Pubchem (https://pubchem.ncbi.nlm.nih.gov/) database. The receptor molecule pdb structures of target proteins were searched in the Research Collaboratory for Structural Bioinformatics Protein Data Bank [33] (RCSB PDB, https://www.rcsb.org/) with the following filtering criteria setting: Source Organism was set to *Homo sapiens*; Experimental Method was set to X-Ray Diffraction; Refinement Resolution $\leq$3; Release Date $\leq$10. Molecular docking was conducted with AutoDock Vina (version 1.2.5) [34,35] to predict the binding affinity and conformation of STDP critical ingredients to the respective targets. The sdf format files of the 13 key ingredients were saved in pdb format through PyMOL (https://www.pymol.org/) and imported into AutoDockTools for assigning atom types and adding atomic charges and saved as molecular docking ligands in pdbqt format. PyMOL was used to remove crystal water and heteroatoms from the receptor molecule and imported into AutoDockTools to assign atom types, add atom charges, and save as molecule-to-acceptor in pdbqt format. The parameters for molecular docking were set thus: ligands were flexible; receptors were rigid; exhaustiveness was set to 32; other parameters were set to default values. For Bax (PDB ID: 4S0O), with the target protein as the center of the grid, the grid size (size x/y/z) and center coordinate (center x/y/z) parameters were adjusted to ensure that the receptor protein was entirely covered by the docking grid. For the other proteins, we used the co-crystal ligand in the PDB structure to identify the protein pocket center coordinates and set the grid size (size 20/20/20). In cases where the binding energy is less than 0 kcal/mol, the receptor is shown to bind spontaneously to the ligand. PyMoL is used to account for the three-dimensional binding interactions of the putative binding mode structures of the receptors and ligands.

### 2.16. Statistical analyses

All data were presented as mean ± standard deviation (SD). ImageJ software was used for image processing, Image Lab 6.0 software was adopted for counting protein bands, and GraphPad Prism 8 software was used for statistical analysis. Differences between groups were analyzed using a one-way analysis of variance and Dunnett's multiple comparison test. A $P$ less than 0.05 was considered to indicate a significant difference.

## 3. Results

### 3.1. STDP treatment reduces myocardial infarct size and enhances cardiac function in AMI rats

We first evaluated the therapeutic effects of STDP in AMI rats by assessing the MI size using TTC staining after 10 days of drug treatment. LAD surgery (Model) caused significant MI in the rat hearts, with an infarct size of 42.1 %, compared with that in rat hearts in the Sham group (Fig. 1A and B). After administration of STDP, the relative mean infarct size of rats in the STDP group was reduced to 18.9 %, which was significantly reduced by 55.1 % in comparison to the rats in the Model group ($P < 0.01$). Furthermore, we evaluated the effects of STDP on cardiac function in AMI rats by analyzing crucial echocardiographic parameters. AMI rats exhibited a significant reduction in left ventricular end-diastolic posterior wall thickness (LVPWd), left ventricular end-systolic posterior wall thickness (LVPWs), left ventricular ejection fraction (LVEF), and left ventricular fractional shortening (LVFS, Fig. 1C and D) compared with that in the Sham group. In contrast, following STDP treatment, LVPWd, LVPWs, LVEF, and LVFS levels were significantly restored in AMI rats compared with those in the Model group rats. In addition, brain natriuretic peptide (BNP), a ventricular hormone, is a highly sensitive and specific marker of changes in ventricular function [36,37]. AMI modeling triggered a marked increase in serum levels of BNP in comparison to the Sham group. In contrast, after STDP administration, there was a significant decrease in the serum levels of BNP in AMI rats (Supplementary Fig. 5). These findings suggest that STDP can effectively reduce MI size and markedly enhance cardiac

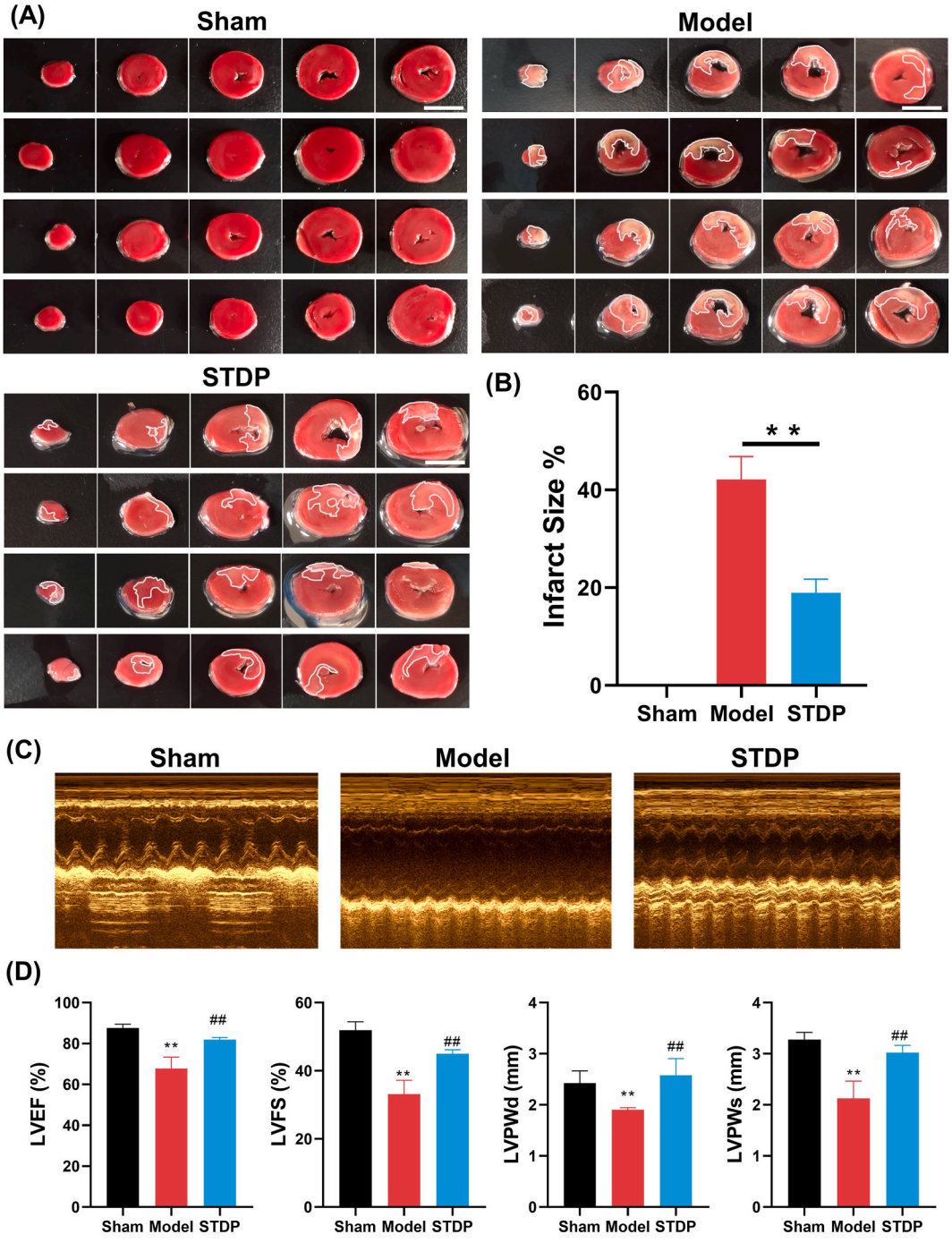


**Fig. 1.** STDP reduces MI size and enhances cardiac function in AMI rats. (A) Representative TTC-stained heart tissue sections. White color: MI area; Red color: non-MI area; Scale (white line): 1 cm. n = 4. (B) Statistics of the relative infarct size of the heart tissue in AMI rats. (C) Representative echocardiogram images. n = 4. (D) Statistics of the key cardiac functional parameters in AMI rats. Compared with the Sham group (Sham), $^{**}P < 0.01$; Compared with the Model group (Model), $^{\#\#}P < 0.01$. STDP: Shexiang-Tongxin dropping pill. (For interpretation of the references to color in this figure legend, the reader is referred to the Web version of this article.)

function in AMI rats, demonstrating its significant therapeutic effect on AMI.

### 3.2. STDP treatment alleviates inflammatory and myocardial injury and inhibits cardiomyocyte apoptosis in AMI rats

The inflammatory response plays a crucial pathophysiological role in AMI, and early intervention studies targeting the IL-1 and IL-6 pathways have shown promising outcomes [38]. Thus, the suppressive effect of STDP on the inflammatory response elicited by the AMI

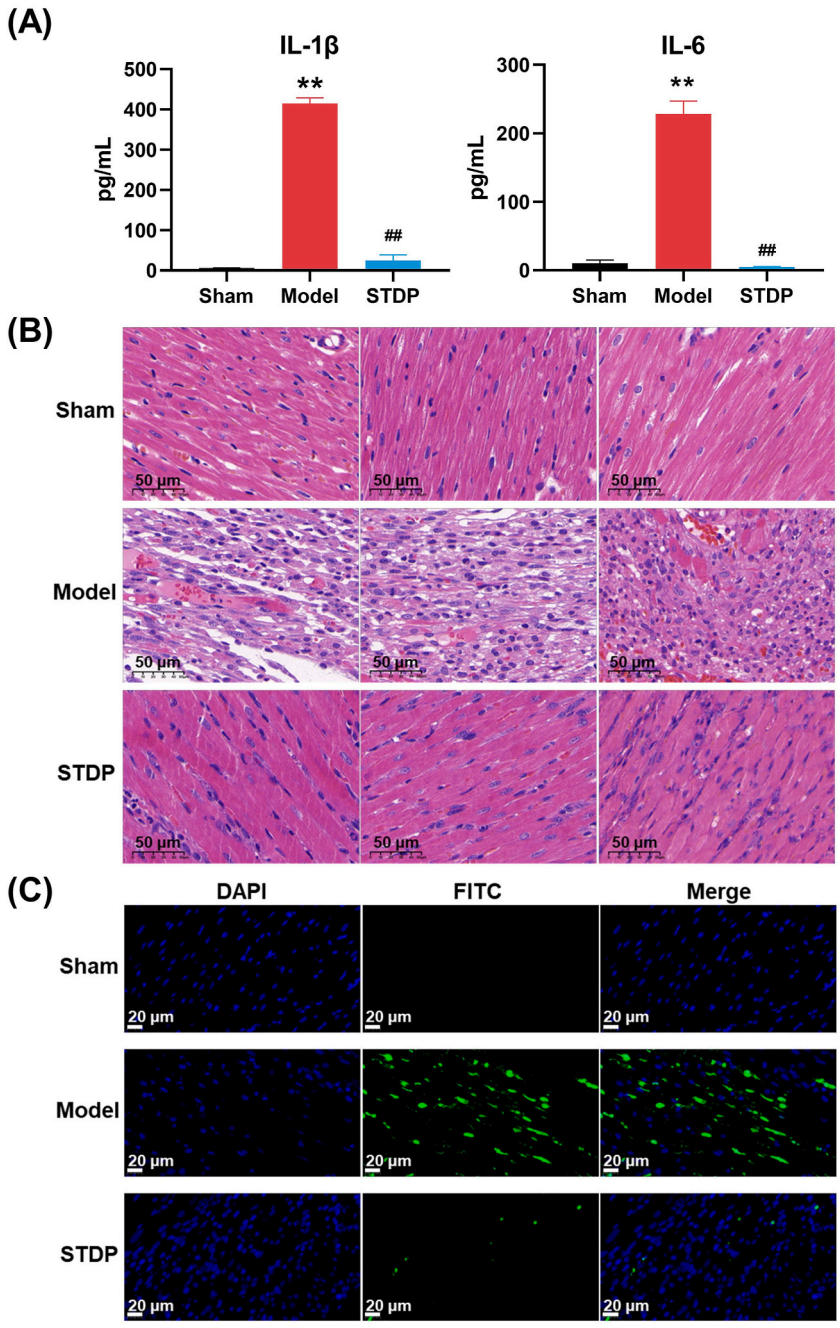


**Fig. 2.** STDP reduces inflammatory and cardiac injury, and cardiomyocyte apoptosis in AMI rats. (A) The serum IL-1β and IL-6 levels in AMI rats. (B) Representative HE-stained sections of the left ventricle of AMI rats after 10 days of STDP treatment, (magnification, × 400), bars = 50 μm. (B) Representative images of TUNEL staining. Images were captured from three randomly selected areas of the left ventricle. Apoptosis of cardiomyocytes in the heart was revealed by yellow-green fluorescence. n = 3, magnification of 400×, bars = 20 μm. Compared with the Sham group (Sham), $^{**}P < 0.01$; Compared with the Model group (Model), $^{\#\#}P < 0.01$. STDP: Shexiang-Tongxin dropping pill. (For interpretation of the references to color in this figure legend, the reader is referred to the Web version of this article.)

model was further examined by measuring the serum IL-1β and IL-6 levels. A significant increase in the serum concentrations of IL-1β and IL-6 was observed in the Model group compared with those in the Sham group ($P < 0.01$) (Fig. 2A). Conversely, STDP treatment resulted in normalized IL-1β and IL-6 levels similar to those observed in the Sham group. These findings indicate that STDP exerted a substantial anti-inflammatory effect in the AMI rats.

Histopathological examination was conducted on the rat heart tissues, and HE staining showed that the myocardial fibers in the Sham group were well-arranged without evident structural changes, and the cytoplasm was uniformly stained. In contrast, the myocardial tissues in the Model group showed structural damage with loosely arranged and broken myocardial fibers, crinkled nuclei, and cytoplasmic vacuolation and edema. The structural damage in the myocardium of AMI rats was significantly improved following STDP treatment (Fig. 2B). Owing to the significance of cardiomyocyte apoptosis in AMI [39], we further investigated the effect of STDP on cardiomyocyte apoptosis in AMI rats using the TUNEL assay. No cardiomyocyte apoptosis was observed in the Sham group, whereas the number of apoptotic cardiomyocytes was increased in the Model group (Fig. 2C). Compared with the Model group, the STDP-treated group exhibited a significant decrease in cardiomyocyte apoptosis, indicating that STDP attenuated the pathological apoptosis of cardiomyocytes in AMI rats. These findings suggest that STDP can reduce pathological changes and inhibit cardiomyocyte apoptosis in AMI.

### *3.3. STDP exerts protective effects against LPS-induced inflammatory injury in RAW264.7 cells and OGD-induced hypoxic injury in HUVECs*

We adopted the LPS-induced inflammation model of RAW264.7 cells to investigate the anti-inflammatory activity of STDP using the nitric oxide release inhibition rate as an indicator. At 25–200 μg/mL, STDP had a dose-dependent inhibitory effect on LPS-induced nitric oxide release from RAW264.7 cells, and the inhibition ratio exceeded 60 % at 200 μg/mL STDP, which was higher than that of the positive drug (Dexamethasone)-treated group (Fig. 3A). This suggests that STDP had a significant anti-inflammatory effect *in vitro*. The OGD model was further used to investigate the effect of STDP in the hypoxia-injured HUVECs. Compared with that of the control group, the cell survival rate of the Model group was approximately 40 %, indicating that the OGD injury model was successfully established (Fig. 3B). Compared with the Model group, 25 μg/mL of STDP significantly improved the HUVECs survival rate after OGD injury, indicating that STDP has a protective effect against hypoxic injury.

### *3.4. STDP treatment restores the transcriptional profile of rat hearts altered by LAD modeling*

The myocardial tissues from the infarcted and normal intersection regions were collected from three rats in each group for transcriptome sequencing. Analysis of the transcriptome sequencing data from the three groups revealed 526 and 131 upregulated and downregulated DEGs, respectively, in the Model group after LAD surgery compared with those in the Sham group (Fig. 4B). Among these DEGs, 175 were commonly significantly induced after STDP treatment, and their expression trends were opposite to those in the Model group, tending toward that in the Control group (Fig. 4C and D). To assess the accuracy of the sequencing data, four DEGs (*Depp1*, *Cd99*, *Nmrk2*, and *Fbxl22*) were subjected to qRT-PCR. qRT-PCR and transcriptome sequencing data showed consistent trends, indicating that transcriptome sequencing data can be used to construct disease networks (Fig. 4E).

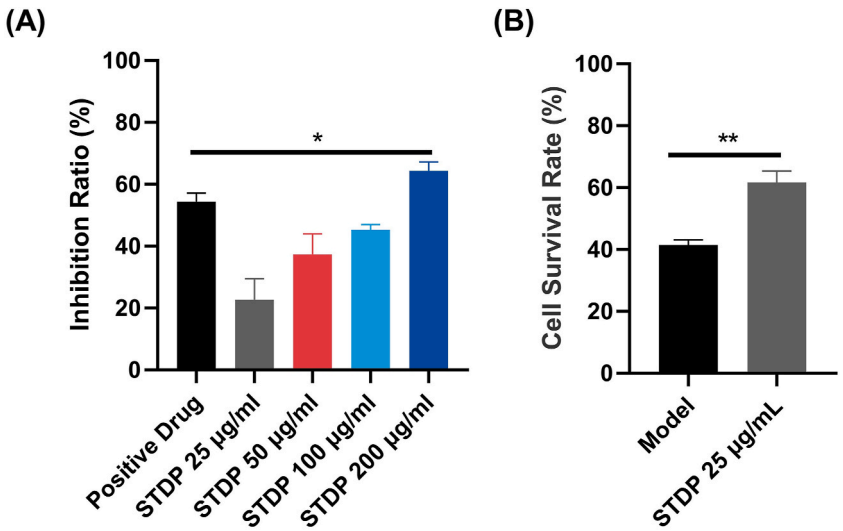


**Fig. 3.** STDP has anti-inflammatory and anti-hypoxic damage effects *in vitro*. (A) The inhibition rate of nitric oxide release from RAW264.7 cells in the LPS-induced inflammation model. (B) HUVECs survival rate after OGD modeling and STDP treatment. Compared with the Positive Drug group, $^{*}P < 0.05$. Compared with the Model group (Model), $^{**}P < 0.01$. n = 3. STDP: Shexiang-Tongxin dropping pill.

### 3.5. STDP treatment restores the AMI disease network

We used whole-transcriptome sequencing combined with a network pharmacology strategy to further analyze the potential pharmacological mechanisms of STDP against AMI. A total of 1641 genes associated with cardiovascular disease in rats were extracted using the Dpylr tool and matched to 34,154 sequenced genes. The resulting common genes were used to construct the AMI network, which comprised 1430 nodes (genes) and 37,291 edges after excluding individual genes with no connections. This indicates that AMI is a complex disease involving multiple targets and multiple pathways. The network was visualized using Cytoscape v3.8.0, and the impact of LAD surgery was visualized by the $Log_2$ (Fold Change) of gene expression in the Sham group vs. Model group after LAD surgery in the established AMI network (Fig. 5A and B). The red and blue nodes indicate upregulation and downregulation of the corresponding gene expression after LAD surgery, respectively (Fig. 5B). The size of the node indicates the importance of the gene in the AMI network, with larger nodes representing more important genes. Pathways closely related to AMI, including apoptosis, MAPK, TGF-β, PI3K, and inflammation pathways, were significantly enriched after LAD surgery (Fig. 5B). The restorative regulatory effect of STDP treatment on genes was marked with EoR (Fig. 5C). Black nodes indicate no regulatory effect of STDP on the gene, while pink

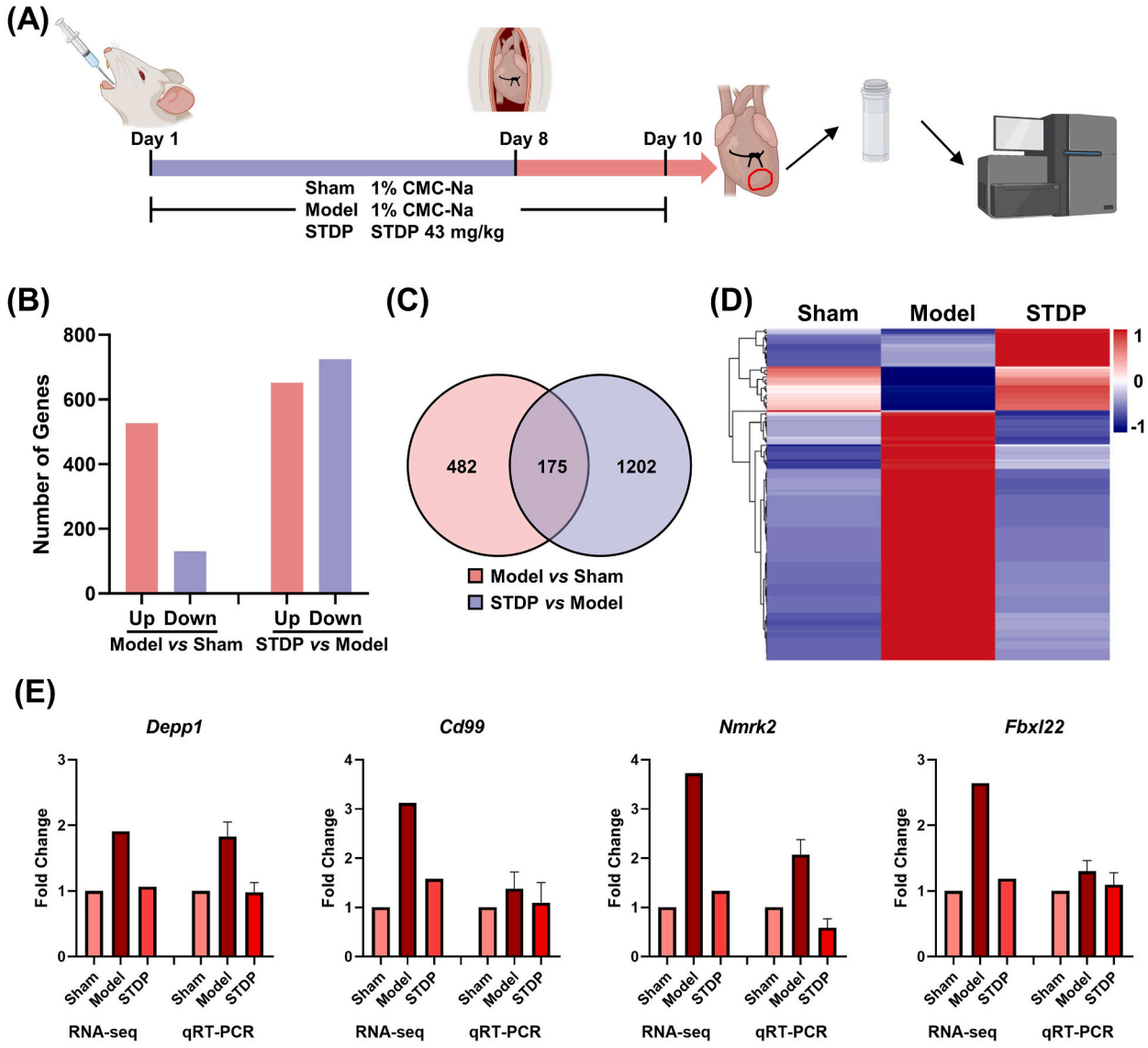


**Fig. 4.** RNA-seq analysis of myocardial tissues obtained from STDP-treated mice with AMI. (A) Experimental procedure. Details are described in the "Materials and Methods" section. (B) Number of upregulated and downregulated DEGs in the Model group *vs* Sham group and the STDP group *vs* Model group. (C) Venn diagram of DEGs between the Model and Sham groups and between the STDP and Model groups. (D) Heat map of 175 genes that were commonly induced after STDP treatment. (E) Gene expression levels of *Depp1*, *Cd99*, *Nmrk2*, and *Fbxl22* were measured by RNA-seq and qRT-PCR. The internal reference was *Actb*, n = 3. STDP: Shexiang-Tongxin dropping pill.

nodes represent a regulatory effect, i.e., EoR >0. The node color gradually increased according to the increased regulatory index EoR. A total of 901 genes were restored after STDP treatment, accounting for 63 % of the disease network. Among these genes, 491 were restored at a rate of ≥80.0 %, indicating that STDP can restate the AMI disease network from an overall perspective.

### 3.6. STDP attenuates AMI in rats predominately through apoptotic and energy metabolic signaling pathways

The topological and transcriptomic parameters of the nodes in the network were combined to extract the key genes that ranked in the top 50 % of the NTRA ranking with EoR >0. A total of 437 genes were selected and subjected to pathway enrichment analysis using

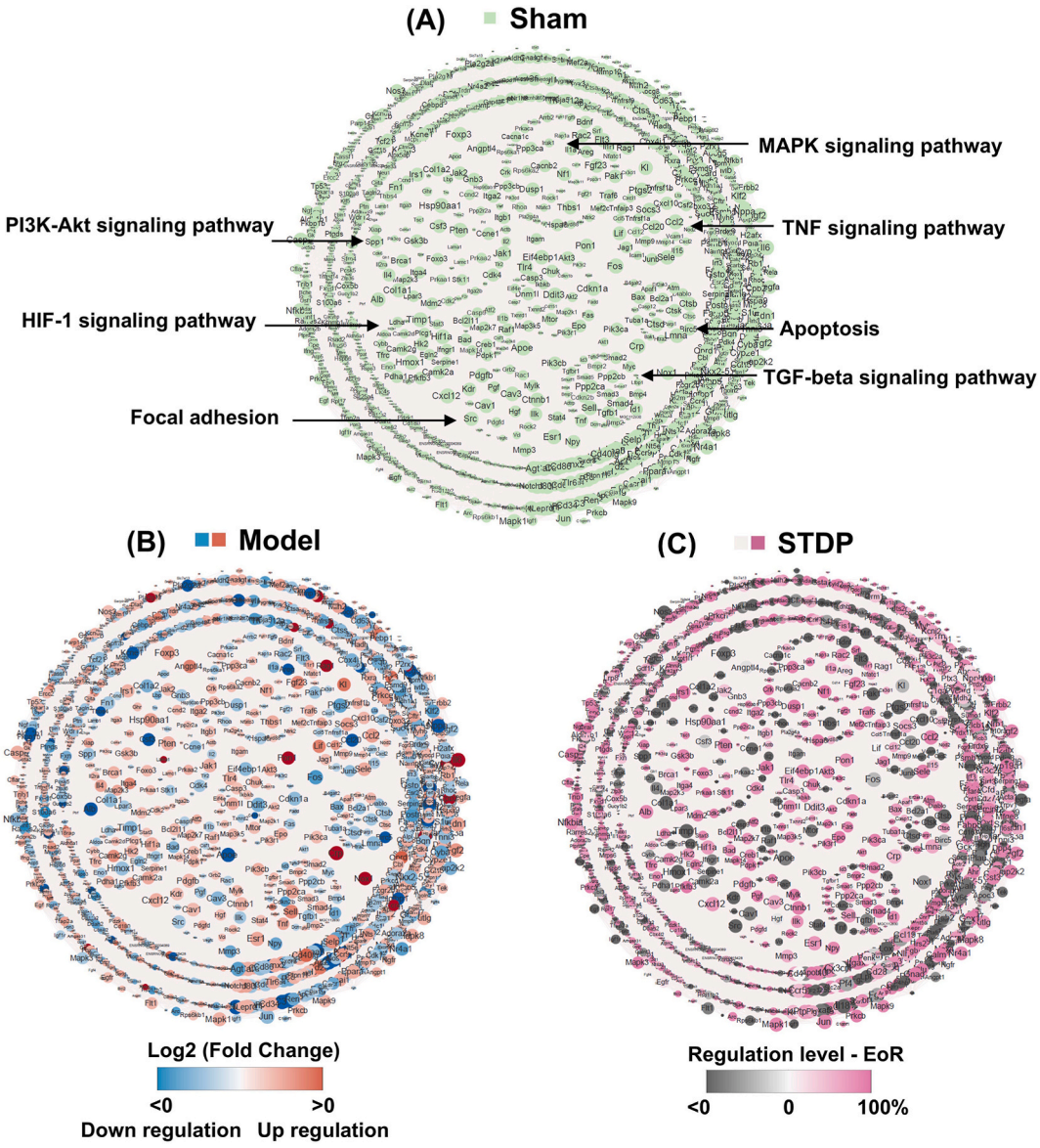


**Fig. 5.** STDP treatment rebalances the AMI network perturbed by LAD surgery. (A) Sham group network. Each node means one gene, and each edge represents the protein-protein interaction relationship between the corresponding proteins of two genes. The size of the nodes is related to the NTRA ranking, and the circles in the network indicate KEGG-enriched critical pathways. (B) LAD surgery perturbs the AMI network, and the nodes in red represent the up-regulation of gene expression after LAD surgery (Log2 Fold Change (Sham/Model) > 0). The blue nodes indicate the down-regulation of gene expression after LAD surgery (Log2 Fold Change (Sham/Model) < 0). The darker color represents the greater change in gene expression. (C) Recovery regulation of AMI network by STDP treatment. The pink node has an EoR >0, indicating that STDP treatment played a restoring role on the gene, and the darker the pink color, the higher the rate of restoring regulation of the gene. Nodes in black indicate no recovery regulation of this gene with STDP treatment. n = 3. STDP: Shexiang-Tongxin dropping pill. (For interpretation of the references to color in this figure legend, the reader is referred to the Web version of this article.)

IPA. A total of 496 pathways were enriched, and the pathways associated with the development of AMI, such as apoptosis and energy metabolism, were significantly enriched (Fig. 6A). Further analysis of essential genes in these pathways revealed that those related to the MAPK and apoptosis signaling pathways were greatly affected. The ERK/MAPK and apoptosis-related signaling pathways were also significantly enriched after STDP treatment, suggesting that ERK/MAPK and apoptosis pathways may be an important mechanism of STDP against AMI. Metascape was further used for biological functional analysis, and the results showed that STDP may act as an anti-AMI agent by regulating apoptosis, inflammation, MAPK, and angiogenesis signaling pathways (Fig. 6B). The crucial genes associated with AMI, including *Fas*, *Stat3*, *Gsk-3β*, and *Foxo3*, were significantly affected in the top 25 enriched pathways identified through IPA. These genes were notably restored after STDP administration with EoR values > 85 % (Supplementary Tables S2 and 3).

### 3.7. STDP mediates anti-AMI effects by inhibiting the apoptosis and ERK/MAPK pathways

The pathway enrichment analysis and biofunctional analysis revealed that the apoptosis and ERK/MAPK pathways were significantly regulated; therefore, the expression levels of the key proteins in these pathways were verified by western blot. The gene and protein levels of Bax (a pro-apoptotic protein) were significantly upregulated after AMI modeling compared with those in the Sham group, while its expression was significantly downregulated following STDP administration compared with that in the Model group (Fig. 7A and B; Supplementary Figs. 4 and 6), consistent with TUNEL analysis of cardiac tissues. These findings indicate that apoptosis is crucial in the development of AMI [40,41] and that STDP exerts an anti-apoptotic effect by inhibiting Bax expression, which is one of the important mechanisms underlying its therapeutic efficacy in AMI treatment. Furthermore, the phosphorylation level of ERK1/2 protein exhibited a similar trend following STDP treatment, further suggesting that STDP acts as an anti-AMI agent by inhibiting the MAPK pathway.

### 3.8. Tanshinone IIA, salvianolic acid B, salvianolic acid A, and resibufogenin may be the main anti-AMI ingredients in STDP

Thirteen essential ingredients (taurine, taurodeoxycholic acid, gentisic acid, cinobufotalin, bufalin, cinobufagin, resibufogenin, protocatechualdehyde, danshensu, tanshinone IIA, salvianolic acid A, salvianolic acid B, and salvianolic acid D) of STDP were subjected to molecular docking with the key proteins involved in the protective mechanisms of STDP, i.e., Bax (PDB ID: 4S0O), ERK1 (PDB ID: 6GES), and ERK2 (PDB ID: 4QP1). The specific predicted protein binding pocket locations and Grid box sizes are presented in Table 1. The molecular docking analysis of 13 key ingredients with three target proteins using AutoDock Vina is presented in Table 2. Among them, the binding energies of tanshinone IIA, salvianolic acid B, salvianolic acid A, and resibufogenin with Bax (PDB ID: 4S0O) were $< -8$ kcal/mol, and the scores of bindings with ERK1 (PDB ID: 6GES) and ERK2 (PDB ID: 4QP1) were lower than co-crystal ligand in the PDB structure, indicating a relatively high affinity between these four ingredients with the three targets. We used PyMol to visualize the putative binding mode of the receptors and ligands. The binding poses and sites of the interactions between the key active ingredients and the core targets are shown in Fig. 8. Salvianolic acid B established four hydrogen bonds with 4S0O by interacting with the residues Pro43, Pro130, Asn106, and Gln28 (Fig. 8A). Additionally, it formed two hydrogen bonds with 4QP1 through interactions with residues Thr159 and Gly182 (Fig. 8C). In Fig. 8B, Tanshinone IIA and salvianolic acid A showed a good shape complementarity

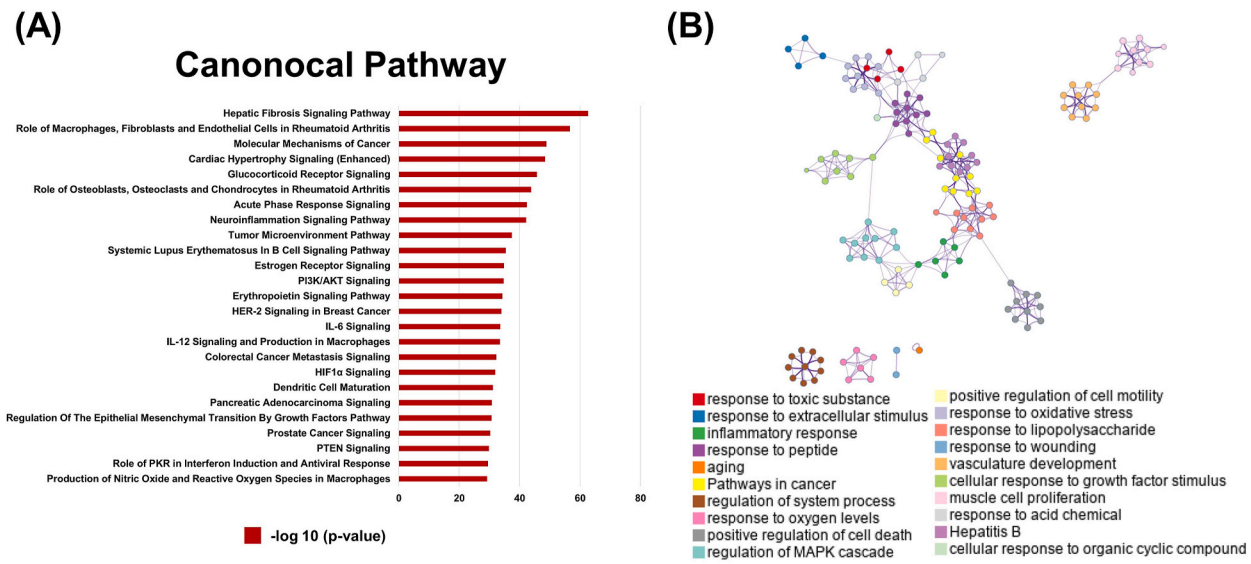


**Fig. 6.** STDP attenuates AMI in rats predominately through apoptotic and energy metabolic signaling pathways. (A) The top 25 pathways were significantly enriched by IPA software under the NTRA and EoR methods. (B) Results of biological function analysis of the recovery regulation genes after STDP treatment. These colors represent different pathways in action, and pathways with the same nodes of action are close to each other. (For interpretation of the references to color in this figure legend, the reader is referred to the Web version of this article.)

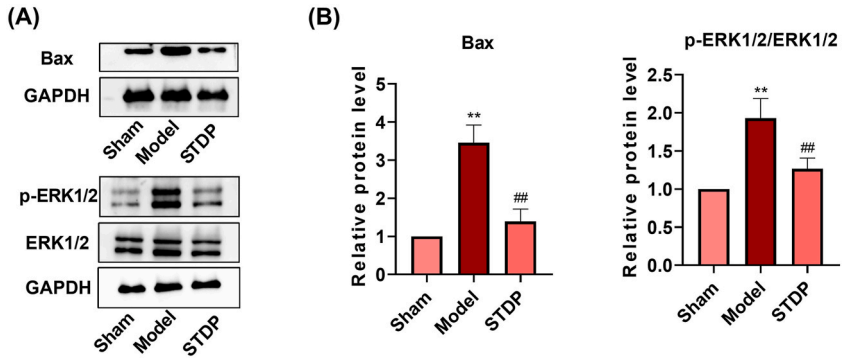


**Fig. 7.** STDP protects rats from AMI by down-regulating apoptosis and ERK/MAPK pathway. (A) Protein expression levels of Bax, p-ERK1/2, and ERK1/2 in rat heart tissue. GAPDH was used as an internal reference (Supplementary Fig. 6). (B) Results of quantitative analysis of western blot images using Image Lab software. Compared with the Sham group (Sham), $^{**}P < 0.01$; Compared with the Model group (Model), $^{\#\#}P < 0.01$. STDP: Shexiang-Tongxin dropping pill.

**Table 1**
Target gene protein pocket coordinates and grid box sizes.

| Target gene | PDB ID | Protein pocket coordinates | Grid box size |
|---|---|---|---|
| Bax | 4S0O | X = 20.67, Y = −0.17, Z = 16.31 | X = 41, Y = 41, Z = 41 |
| ERK1 | 6GES | X = 31.37, Y = −12.20, Z = −14.20 | X = 20, Y = 20, Z = 20 |
| ERK2 | 4QP1 | X = −25.01, Y = −32.27, Z = −43.91 | X = 20, Y = 20, Z = 20 |

**Table 2**
Molecular docking affinity values for binding of major ingredients to core targets.

| Protein / Affinity kcal/mol / Compound | 4S0O | 6GES | 4QP1 |
|---|---|---|---|
| Tanshinone IIA | −9.1 | −9.4 | −7.4 |
| Salvianolic acid B | −8.8 | −8.4 | −8.6 |
| Salvianolic acid A | −8.4 | −8.7 | −8.2 |
| Resibufogenin | −8.3 | −8.7 | −7.5 |
| Salvianolic acid D | −7.5 | −8.6 | −7.5 |
| Taurodeoxycholic acid | −8.2 | −7.7 | −7.0 |
| Bufalin | −8.0 | −7.9 | −7.8 |
| Cinobufotalin | −8.0 | −6.0 | −7.2 |
| Cinobufagin | −7.5 | −8.2 | −7.5 |
| Danshensu | −6.3 | −6.3 | −5.7 |
| Gentisic acid | −5.7 | −5.4 | −5.1 |
| Protocatechualdehyde | −5.4 | −5.3 | −5.0 |
| Taurine | −4.0 | −3.3 | −3.5 |

with the binding pocket of 6GES protein and exhibited high affinity. Resibufogenin formed three hydrogen bonds with 6GES by interacting with the residues Met125, Lys131, and Ser170 (Fig. 8B). These indicate that tanshinone IIA, salvianolic acid A, salvianolic acid B, and resibufogenin may be the main pharmacodynamic substances of STDP for anti-AMI.

## 4. Discussion

AMI is the most critical manifestation of coronary artery disease [1]. Although the prognosis of AMI has improved significantly in the past decade, it continues to be the predominant source of morbidity and mortality worldwide. After AMI, the affected myocardium undergoes hypoxia and apoptosis, triggering an inflammatory response; this sustained inflammation causes collagen accumulation, resulting in cardiac remodeling and heart failure [42,43]. PPCI and coronary artery bypass grafting are the most common clinical treatments for AMI currently; however, they may cause critical complications, such as bleeding and ischemia-reperfusion injury [44]. Meanwhile, the single-target immunotherapy against post-MI inflammatory response showed no significant improvement in MI size and clinical outcome [3], prompting the identification of safer multi-targeted drugs. Clinical studies have demonstrated that STDP can effectively attenuate myocardial injury and cardiac pathological remodeling caused by myocardial ischemia-reperfusion after AMI, revealing its potential and safety in treating AMI [45]. However, the molecular mechanism of STDP against AMI remains elusive. To

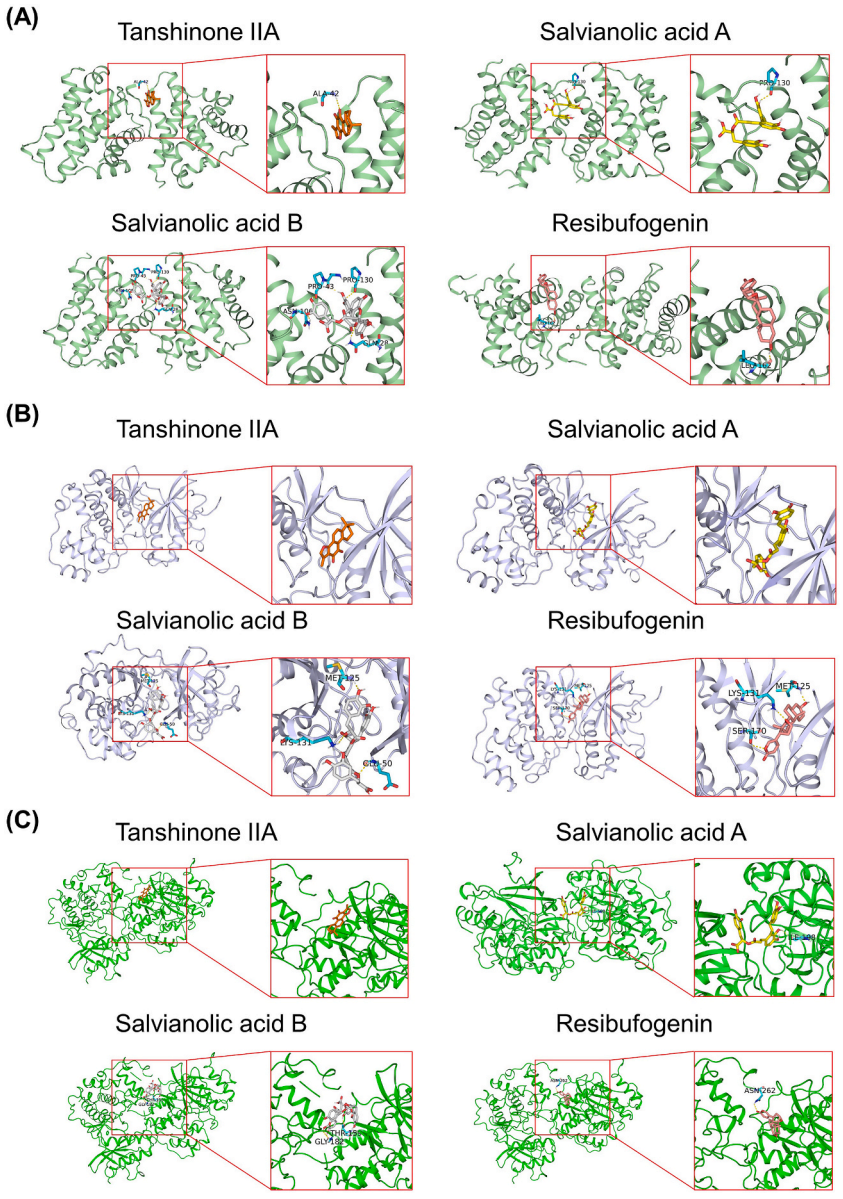


**Fig. 8.** Docking poses of Tanshinone IIA, Salvianolic acid B, Salvianolic acid A, and Resibufogenin with three core targets. (A) Bax-Tanshinone IIA, Bax-Salvianolic acid A, Bax-Salvianolic acid B, and Bax-Resibufogenin. (B) ERK1-Tanshinone IIA, ERK1-Salvianolic acid A, ERK1-Salvianolic acid B, and ERK1-Resibufogenin. (C) ERK2-Tanshinone IIA, ERK2-Salvianolic acid A, ERK2-Salvianolic acid B, and ERK2-Resibufogenin.

explore the molecular mechanism of STDP against AMI, its pharmacodynamic effects in treating AMI were evaluated *in vitro* and *in vivo* using HUVECs oxygen-glucose deprivation, RAW264.7 cell inflammatory injury, and rat LAD surgery models. Subsequently, the whole transcriptome gene sequencing technology and network pharmacology analysis were integrated to elucidate the molecular mechanism of STDP against AMI. Finally, we performed molecular docking to identify the key anti-AMI ingredients in STDP.

In this study, STDP improved cardiac function, reduced myocardial infarct size, and exerted substantial protective effects against LAD-induced AMI diversely. These include the reduction of inflammation response, mitigation of cardiac tissue structural damage, and attenuation of cardiomyocyte apoptosis in AMI rats. Meanwhile, *in vitro*, STDP also exerted anti-inflammatory damage and anti-cellular hypoxic injury effects. Further analysis of whole-transcriptome sequencing data from experimental rat hearts using a network pharmacology approach revealed that STDP could provide anti-AMI effects through multiple targets, and 63 % of the dys-regulated genes after AMI were restored after STDP treatment, with more than half of them recovered at the rate of >80 %. Integrated pathway enrichment analysis, biofunctional analysis, and *in vivo* validation experiments showed that the inhibition of apoptosis and ERK/MAPK pathways by reducing the expression levels of Bax and p-ERK1/2 may be an important mechanism of STDP against AMI. Molecular docking of these three core proteins with 13 key ingredients in the STDP revealed that tanshinone IIA, salvianolic acid A,

salvianolic acid B, and resibufogenin have high affinity with Bax, ERK1, and ERK2. These results suggest that tanshinone IIA, salvianolic acid A, salvianolic acid B, and resibufogenin are the primary pharmacodynamic substances of STDP in AMI treatment by targeting Bax and ERK1/2.

Apoptosis is a major contributor to myocardial injury after AMI [28] and mediates post-MI myocardial cell death, left ventricular remodeling, and heart failure [29]. Bax overexpression in human post-MI cardiomyocytes accelerated cellular injury after MI [46]. Moreover, *Fas* expression was positively correlated with apoptosis activation [28]. *Bax* and *Fas* downregulation, *Bcl-2* upregulation, and increased Bcl-2/Bax ratio attenuated cardiomyocyte apoptosis after AMI [47]. STAT3, a crucial factor in the JAK/STAT (IL-6) signaling pathway, and phosphorylated STAT3 protein expression levels, were significantly reduced in the myocardium of MI rats after JAK2 inhibitor treatment. Meanwhile, the Bax protein expression level was increased, indicating that the JAK/STAT pathway was involved in post-MI cardiomyocyte apoptosis [48]. Similarly, according to a report, STDP could protect the heart from pituitrin-induced myocardial ischemic injury through an anti-apoptotic effect [16]. Our study confirmed these findings, as TUNEL staining showed that STDP attenuated the pathological apoptosis of cardiomyocytes in AMI rats, and topological and transcriptomic sequencing also revealed that *Bax*, *Bcl-2*, and *Stat3* mRNAs and Bax protein were significantly increased in the heart tissue of AMI rats after LAD surgery. After STDP intervention, the recovery regulation efficiency of *Bax*, *Bcl-2*, and *Stat3* were 72.05 %, 94.19 %, and 85.83 % (Supplementary Table S3), respectively. These findings demonstrate that STDP inhibited Bax expression and exerted an anti-apoptotic effect, which was a crucial mechanism for its therapeutic efficacy in AMI treatment.

Previous studies showed that reduced ERK1/2 protein expression after AMI improved cardiac function in rats and that MAPK signaling pathway inhibition attenuated ISO-induced myocardial injury, implying that ERK/MAPK signaling pathway inhibition could prevent cardiomyocyte apoptosis [49,50]. Similarly, the protective effect of STDP against ISO-induced myocardial injury was reportedly related to the ERK1/2 signaling pathway [17]. ERK1/2 mediated M1-polarized macrophage chemotaxis and inflammatory cytokine production in an MI mouse model, suggesting that ERK1/2 was involved in the inflammatory response after MI [51]. In our study, p-ERK1/2 protein expression levels were increased in the heart tissues of AMI rats after LAD surgery, while STDP decreased p-ERK1/2 protein expression levels, indicating that STDP might play a myocardial protective role in AMI by inhibiting the ERK/MAPK signaling pathway.

In addition, we established a "compound-target network" between the 13 key ingredients in STDP and genes that showed recovery of regulation after STDP treatment (Supplementary Fig. 3). The potential targets of these ingredients were predicted through the PharmMapper database [52–54] and got a total of 434 potential target genes. Subsequently, we took the intersection of these genes with the 901 genes with EoR >0 and obtained 107 genes. The 107 genes were further used to construct the "compound-target" network. Further pathway analysis showed that these genes were mainly involved in the pathways of lipid and atherosclerosis, regulation of inflammatory response, and regulation of apoptotic signaling. These pathways are known to play an important role in the development of AMI and show a recovery regulation trend after STDP treatment.

In addition to the pathways associated with disease phenotypes, STDP intervention significantly enriched the PI3K/Akt pathway (Fig. 6A), which is a critical mechanism in the onset, progression, and treatment of MI. Its downstream molecules, glycogen synthase kinase 3β (GSK-3β) and forkhead box O3 (FOXO3), were involved in the protection of cardiac myocytes. The upregulation of GSK-3β and p-GSK-3β expression reportedly activates the PI3K/Akt/GSK-3β signaling pathway to protect the myocardium from AMI injury [55]. GSK-3β is also a key mediator of the inflammatory response and has been implicated in various cardiac diseases. GSK-3β could directly mediate the activation of the NLRP3 inflammasome, which in turn leads to cardiac dysfunction in MI [56]. *Foxo3a* activation could promote resistance to oxidative stress and reduce MI [51]. FOXO3 could also promote antigen-presenting cells to express and secrete IL-10, IL-33, and IL-34, establishing a regulatory T cell (Treg)-inducing niche in the mediastinal lymph node. After myocardial deployment, Tregs contribute to the reduction of inflammation following MI and cardiac repair [57]. Similarly, this study showed that the expression levels of *Gsk-3β* and *Foxo3a* were decreased in the rat heart after LAD surgery, and after STDP administration, their expression was restored by 91.41 % and 88.61 %, respectively (Supplementary Table S3). Notably, along with the key targets highlighted above, STDP may also benefit AMI therapy through several newly discovered anti-AMI targets. Lysine demethylase 3A (KDM3A), also known as Jumonji domain-containing 1A, performs various biological functions, such as positive regulation of gene expression and response to hypoxia. KDM3A overexpression can improve cardiac function, attenuate cardiac oxidative stress and pathological changes, and protect the myocardium from AMI-induced injury [58]. TBC1 domain family member 15 (TBC1D15) mRNA/protein levels were downregulated in human ischemic cardiomyopathy or MI samples [59], and high TBC1D15 expression restored lysosomal degradation by binding to mitochondrial *Fis1* and promoting the clearance of damaged mitochondria, helping the heart retain myocardial mitochondrial function and integrity and protecting cardiac contractile function [60]. TBC1D15 could also recruit *Drp1* to the mitochondrial-lysosome contact sites and bind to *Drp1* to promote asymmetric mitochondrial fission and clearance to preserve mitochondrial integrity [60]. These imply that TBC1D15 may be an ideal new target for treating MI. ATP synthase inhibitory factor subunit 1 (ATPIF1), a protein that inhibits ATP hydrolysis through the reverse function of ATP synthase during myocardial ischemia, is significantly upregulated in LAD surgery-induced MI cardiomyocytes, and ATPIF1 knockdown resulted in a significant reduction in the expression level of glycolytic pathway proteins in the heart after MI and improved pathological remodeling of the heart by promoting metabolic reprogramming [61]. Dachshund family transcription factor 1 (*Dach1*) is expressed in embryonic and adult coronary endothelial cells. Overexpressed *Dach1* enhanced normal arterial differentiation, increasing the number of arteries after MI and extending arterial branching, which could promote recovery from ischemic injury and improve survival and cardiac function after MI, serving as a potential therapeutic MI target for enhancing ischemic cardiac revascularization [62]. After STDP treatment, the recovery regulation rates of these four newly identified targets were 82.7 % (*Kdm3a*), 92.4 % (*Tbc1d15*), 85.6 % (*Atpif1*), and 78.2 % (*Dach1*) (Supplementary Table S4), respectively. These findings suggest that STDP, a common clinical drug for AMI, is highly effective and can play a comprehensive role in treating AMI. Additionally, STDP may exert its benefits by targeting newly

identified AMI targets, such as KDM3A, TBC1D15, ATPIF1, and *Dach1*.

## 5. Conclusions

Our study demonstrated that the anti-AMI effects of STDP primarily involve the reduction of myocardial infarct size, enhancement of cardiac function, reduction of inflammatory response, attenuation of cardiac pathological changes, and inhibition of cardiomyocyte apoptosis. The protective effects of STDP against LPS-induced inflammatory injury and OGD-induced hypoxic injury were also demonstrated *in vitro*. Integrating network pharmacology analysis with whole transcriptome sequencing data revealed that STDP restored 63 % of the AMI disease network. Additionally, inhibiting apoptosis by decreasing Bax expression levels and reducing the activity of the ERK/MAPK pathway by reducing p-ERK1/2 expression levels may be the crucial mechanisms underlying the anti-AMI effects of STDP. Tanshinone IIA, salvianolic acid A, salvianolic acid B, and resibufogenin may be the main pharmacodynamic substances of STDP in the treatment of AMI by targeting Bax and ERK1/2. Overall, our results suggest that STDP can exert therapeutic effects in AMI through multiple targets and pathways.

## CRediT authorship contribution statement

**Jun Yan:** Writing – review & editing, Writing – original draft, Visualization, Validation, Formal analysis. **Hanbing Liu:** Writing – original draft, Methodology, Formal analysis. **Jiaxin Shang:** Writing – review & editing, Visualization, Formal analysis. **Qianqian Fang:** Project administration, Conceptualization. **Jianfeng Ye:** Project administration, Conceptualization. **Xiaoyan Lu:** Writing – review & editing, Supervision, Project administration, Methodology, Conceptualization. **Xiaohui Fan:** Supervision, Project administration, Methodology, Funding acquisition, Conceptualization.

## Ethical approval statement

The animal experimental design and protocols adopted in this study were reviewed and approved by the Animal Care and Use Committee of Zhejiang University School of Medicine (ZJU20230308).

## Data availability statement

Data will be made available on request.

## Funding

This study was supported by the “Pioneer” and “Leading Goose” R&D Program of Zhejiang (No. 2024C03106) and the Fundamental Research Funds for the Central Universities (No. 226-2024-00001).

## Declaration of competing interest

The authors declare that they have no known competing financial interests or personal relationships that could have appeared to influence the work reported in this paper.

## Abbreviations

| | |
|---|---|
| AMI | acute myocardial infarction |
| STDP | Shexiang-Tongxin dropping pill |
| MI | myocardial infarction |
| PPCI | primary percutaneous coronary intervention |
| TCM | Traditional Chinese Medicine; |
| ISO | isoproterenol |
| LAD | left anterior descending |
| LVPWd | left ventricular end-diastolic posterior wall thickness |
| LVPWs | left ventricular end-systolic posterior wall thickness |
| LVEF | left ventricular ejection fraction |
| LVFS | left ventricular fractional shortening |
| ELISA | Enzyme-linked immunosorbent assay |
| TTC | triphenyl tetrazolium chloride |
| HE | hematoxylin-eosin |
| TUNEL | terminal deoxynucleotidyl transferase-mediated dNTP nick end labeling |
| HUVECs | Human umbilical vein endothelial cells |
| DMEM | Dulbecco’s modified Eagle’s medium |
| LPS | lipopolysaccharide |

| | |
|---|---|
| CCK-8 | Cell counting kit-8 |
| OGD | oxygen-glucose deprivation |
| DEGs | differentially expressed genes |
| KEGG | Kyoto encyclopedia of genes and genomes |
| NTRA | network topology and transcriptomics-based approach |
| EoR | efficiency of recovery regulation |
| RL | regulation level |
| IPA | ingenuity pathways analysis |
| qRT-PCR | quantitative real-time PCR |
| RIPA | radioimmunoprecipitation assay |
| PMSF | phenylmethanesulfonyl fluoride |
| PVDF | polyvinylidene fluoride |
| RCSB PDB | RCSB Protein Data Bank |
| SD | standard deviation |
| GSK-3β | glycogen synthase kinase 3β |
| FOXO3 | forkhead box O3 |
| KDM3A | lysine demethylase 3A |
| TBC1D15 | TBC1 domain family member 15 |
| ATPIF1 | ATP synthase inhibitory factor subunit 1 |
| *Dach1* | Dachshund family transcription factor 1 |

## Appendix A. Supplementary data

Supplementary data to this article can be found online at https://doi.org/10.1016/j.heliyon.2024.e39939.

## References


[1] G.W. Reed, J.E. Rossi, C.P. Cannon, Acute myocardial infarction, Lancet 389 (10065) (2017) 197–210, https://doi.org/10.1016/S0140-6736(16)30677-8.

[2] M.F.M. Fathil, M.K. Md Arshad, S.C.B. Gopinath, U. Hashim, R. Adzhri, R.M. Ayub, A.R. Ruslinda, M. Nuzaihan, M. N, A.H. Azman, M. Zaki, T. Tang, Diagnostics on acute myocardial infarction: cardiac troponin biomarkers, Biosens. Bioelectron. 70 (2015) 209–220, https://doi.org/10.1016/j.bios.2015.03.037.

[3] S. Ong, S. Hernández-Reséndiz, G.E. Crespo-Avilan, R.T. Mukhametshina, X. Kwek, H.A. Cabrera-Fuentes, D.J. Hausenloy, Inflammation following acute myocardial infarction: multiple players, dynamic roles, and novel therapeutic opportunities, Pharmacol. Ther. 186 (2018) 73–87, https://doi.org/10.1016/j.pharmthera.2018.01.001.

[4] F. Pedersen, V. Butrymovich, H. Kelbæk, K. Wachtell, S. Helqvist, J. Kastrup, L. Holmvang, P. Clemmensen, T. Engstrøm, P. Grande, K. Saunamäki, E. Jørgensen, Short- and long-term cause of death in patients treated with primary PCI for STEMI, J. Am. Coll. Cardiol. 64 (20) (2014) 2101–2108, https://doi.org/10.1016/j.jacc.2014.08.037.

[5] M.F. Piepoli, U. Corrà, P. Dendale, I. Frederix, E. Prescott, J.P. Schmid, M. Cupples, C. Deaton, P. Doherty, P. Giannuzzi, I. Graham, T.B. Hansen, C. Jennings, U. Landmesser, P. Marques-Vidal, C. Vrints, D. Walker, H. Bueno, D. Fitzsimons, A. Pelliccia, Challenges in secondary prevention after acute myocardial infarction: a call for action, Eur. J. Prev. Cardiol. 23 (18) (2016) 1994–2006, https://doi.org/10.1177/2047487316663873.

[6] B. Pitt, R. Ferrari, M. Gheorghiade, D.J. van Veldhuisen, H. Krum, J. Mcmurray, J. Lopez-Sendon, Aldosterone blockade in post-acute myocardial infarction heart failure, Clin. Cardiol. 29 (10) (2006) 434–438, https://doi.org/10.1002/clc.4960291004.

[7] Y.J. Shimada, R.P. Giugliano, Emerging antithrombotic drugs for acute coronary syndrome, Expert Opin Emerg, Drugs 18 (3) (2013) 307–318, https://doi.org/10.1517/14728214.2013.819342.

[8] A. Abbate, B.W. Van Tassell, G. Biondi-Zoccai, M.C. Kontos, J.D. Grizzard, D.W. Spillman, C. Oddi, C.S. Roberts, R.D. Melchior, G.H. Mueller, N.A. Abouzaki, L. R. Rengel, A. Varma, M.L. Gambill, R.A. Falcao, N.F. Voelkel, C.A. Dinarello, G.W. Vetrovec, Effects of interleukin-1 blockade with anakinra on adverse cardiac remodeling and heart failure after acute myocardial infarction [from the Virginia commonwealth university-anakinra remodeling trial (2) (VCU-ART2) pilot study], Am. J. of Cardio. 111 (10) (2013) 1394–1400, https://doi.org/10.1016/j.amjcard.2013.01.287.

[9] K.W. Baran, M. Nguyen, G.R. Mckendall, C.T. Lambrew, G. Dykstra, S.T. Palmeri, R.J. Gibbons, S. Borzak, B.E. Sobel, S.G. Gourlay, A.C. Rundle, C.M. Gibson, H. V. Barron, Double-blind, randomized trial of an anti-CD18 antibody in conjunction with recombinant tissue plasminogen activator for acute myocardial infarction, Circulation 104 (23) (2001) 2778–2783, https://doi.org/10.1161/hc4801.100236.

[10] O. Kleveland, G. Kunszt, M. Bratlie, T. Ueland, K. Broch, E. Holte, A.E. Michelsen, B. Bendz, B.H. Amundsen, T. Espevik, S. Aakhus, J.K. Damås, P. Aukrust, R. Wiseth, L. Gullestad, Effect of a single dose of the interleukin-6 receptor antagonist tocilizumab on inflammation and troponin T release in patients with non-ST-elevation myocardial infarction: a double-blind, randomized, placebo-controlled phase 2 trial, Eur. Heart J. 37 (30) (2016) 2406–2413, https://doi.org/10.1093/eurheartj/ehw171.

[11] Y. Lu, X. Chu, J. Zhang, Y. Zhao, C. Jin, J. Zhu, G. Fu, F. Qiu, Effect of Shexiang Tongxin dropping pill on stable coronary artery disease patients with normal fractional flow reserve and coronary microvascular disease: a study protocol, Medicine (Baltim.) 99 (38) (2020) e22126, https://doi.org/10.1097/MD.0000000000022126.

[12] D. Chen, S. Lin, W. Xu, M. Huang, J. Chu, F. Xiao, J. Lin, J. Peng, Qualitative and quantitative analysis of the major constituents in shexiang tongxin dropping pill by HPLC-Q-TOF-MS/MS and UPLC-QQQ-MS/MS, Molecules 20 (10) (2015) 18597–18619, https://doi.org/10.3390/molecules201018597.

[13] S. Han, X. Zhang, L. Zhang, H. Shang, Clinical evidence evaluation of Shexiang Tongxin dropping pill for slow blood flow after PCI, Modernization of Traditional Chin, Med. Mate. Medica-World Sci. Technol. (20) (2018) 1772–1777.

[14] Y. Zheng, B. Deng, W. Zheng, L. Sheng, G. Li, N. Tang, Beneficial effects of she Xiang tong xin dropping pill on cytokines and left ventricular function in patients with acute myocardial infarction undergoing primary percutaneous coronary intervention, International Journal of Cardiovascular Disease 48 (2) (2021) 116–119.

[15] Y. Yao, Z. Zeng, Y. Zhao, T. Li, Y. Liu, R. Chen, Effect of Shexiang Tongxin dripping pills on coronary microcirculation disorder and cardiacdysfunction in a porcine model of myocardial ischemia-reperfusion injury, J. South. Med. Univ. 40 (6) (2020) 899–906, https://doi.org/10.12122/j.issn.1673-4254.2020.06.19.

[16] S. Lin, J. Chu, L. Zhang, D. Chen, F. Xiao, H. Chen, J. Lin, Y. Chen, Y. Zhu, J. Peng, Protective effects of Shexiang Tongxin dropping pill on pituitrin-induced acute myocardial ischemia in rats, Mol. Med. Rep. 16 (3) (2017) 3125–3132, https://doi.org/10.3892/mmr.2017.6963.

[17] J. Qi, W. Pan, Y. Tan, J. Luo, D. Fan, J. Yu, J. Wu, M. Zhang, Shexiang tongxin dropping pill protects against isoproterenol-induced myocardial ischemia *in vivo* and *in vitro*, Oncotarget 8 (65) (2017) 108958–108969, https://doi.org/10.18632/oncotarget.22440.

[18] M. Kibble, N. Saarinen, J. Tang, K. Wennerberg, S. Mäkelä, T. Aittokallio, Network pharmacology applications to map the unexplored target space and therapeutic potential of natural products, Nat. Prod. Rep. 32 (8) (2015) 1249–1266, https://doi.org/10.1039/c5np00005j.

[19] B. Huang, J. Xiong, X. Zhao, Y. Zheng, N. Zhu, Network pharmacology-based analysis of the pharmacological mechanisms of aloperine on cardiovascular disease, Evid. Based Complement, Altern. Med. 2020 (2020) 1–8, https://doi.org/10.1155/2020/5180716.

[20] J. Liao, C. Hao, W. Huang, X. Shao, Y. Song, L. Liu, N. Ai, X. Fan, Network pharmacology study reveals energy metabolism and apoptosis pathways-mediated cardioprotective effects of Shenqi Fuzheng, J. Ethnopharmacol. 227 (2018) 155–165, https://doi.org/10.1016/j.jep.2018.08.029.

[21] L. Chen, Y. Cao, H. Zhang, D. Lv, Y. Zhao, Y. Liu, G. Ye, Y. Chai, Network pharmacology-based strategy for predicting active ingredients and potential targets of Yangxinshi tablet for treating heart failure, J. Ethnopharmacol. 219 (2018) 359–368, https://doi.org/10.1016/j.jep.2017.12.011.

[22] X. Li, L. Wu, W. Liu, Y. Jin, Q. Chen, L. Wang, X. Fan, Z. Li, Y. Cheng, C. Chan, A network pharmacology study of Chinese medicine QiShenYiQi to reveal its underlying multi-compound, multi-target, multi-pathway mode of action, PLoS One 9 (5) (2014) e95004, https://doi.org/10.1371/journal.pone.0095004.

[23] X. Chang, Y. Li, J. Liu, Y. Wang, X. Guan, Q. Wu, Y. Zhou, X. Zhang, Y. Chen, Y. Huang, R. Liu, β-tubulin contributes to Tongyang Huoxue decoction-induced protection against hypoxia/reoxygenation-induced injury of sinoatrial node cells through SIRT1-mediated regulation of mitochondrial quality surveillance, Phytomedicine 108 (2023) 154502, https://doi.org/10.1016/j.phymed.2022.154502.

[24] L. Wang, Z. Li, X. Zhao, W. Liu, Y. Liu, J. Yang, X. Li, X. Fan, Y. Cheng, L. Ke, K. Liu, A network study of Chinese medicine xuesaitong injection to elucidate a complex mode of action with multicompound, multitarget, and multipathway, Evid Based Complement, Altern. Med. 2013 (2013) 652373–652378, https://doi.org/10.1155/2013/652373.

[25] W. Guo, J. Huang, N. Wang, H. Tan, F. Cheung, F. Chen, Y. Feng, Integrating network pharmacology and pharmacological evaluation for deciphering the action mechanism of herbal formula Zuojin pill in suppressing hepatocellular carcinoma, Front. Pharmacol. 10 (2019) 1185, https://doi.org/10.3389/fphar.2019.01185.

[26] S. Zhang, H. Liu, Q. Fang, H. He, X. Lu, Y. Wang, X. Fan, Shexiang tongxin dropping pill protects against chronic heart failure in mice via inhibiting the ERK/MAPK and TGF-β signaling pathways, Front. Pharmacol. 12 (2021) 796354, https://doi.org/10.3389/fphar.2021.796354.

[27] A.B. Nair, S. Jacob, A simple practice guide for dose conversion between animals and human, J. Basic Clin. Pharm. 7 (2) (2016) 27–31, https://doi.org/10.4103/0976-0105.177703.

[28] J. Kajstura, W. Cheng, K. Reiss, W.A. Clark, E.H. Sonnenblick, S. Krajewski, J.C. Reed, G. Olivetti, P. Anversa, Apoptotic and necrotic myocyte cell deaths are independent contributing variables of infarct size in rats, Lab. Invest. 74 (1) (1996) 86.

[29] A. Abbate, G.G.L. Biondi-Zoccai, R. Bussani, A. Dobrina, D. Camilot, F. Feroce, R. Rossiello, F. Baldi, F. Silvestri, L.M. Biasucci, A. Baldi, Increased myocardial apoptosis in patients with unfavorable left ventricular remodeling and early symptomatic post-infarction heart failure, J. Am. Coll. Cardiol. 41 (5) (2003) 753–760, https://doi.org/10.1016/S0735-1097(02)02959-5.

[30] R. Esmaeili, A. Sadeghpour, A. Darbandi-Azar, K. Majidzadeh-A, A. Vajhi, M. Sadeghizadeh, Echocardiographic assessment of myocardial infarction: comparison of a rat model in two strains, Iran, J. Vet. Res. 18 (1) (2017) 30–35.

[31] M. Li, C.M. Yu, L. Cheng, M. Wang, X. Gu, K.H. Lee, T. Wang, Y.T. Sung, J.E. Sanderson, Repair of infarcted myocardium by an extract of geum japonicum with dual effects on angiogenesis and myogenesis, Clin. Chem. 52 (8) (2006) 1460–1468, https://doi.org/10.1373/clinchem.2006.068247.

[32] L. Wu, Y. Wang, Z. Li, B. Zhang, Y. Cheng, X. Fan, Identifying roles of "Jun-Chen-Zuo-Shi" component herbs of QiShenYiQi formula in treating acute myocardial ischemia by network pharmacology, Chin. Med. 9 (1) (2014) 24, https://doi.org/10.1186/1749-8546-9-24.

[33] H.M. Berman, The protein data bank, Nucleic Acids Res. 28 (1) (2000) 235–242, https://doi.org/10.1093/nar/28.1.235.

[34] J. Eberhardt, D. Santos-Martins, A.F. Tillack, S. Forli, Autodock vina 1.2.0: new docking methods, expanded force field, and python bindings, J. Chem. Inf. Model. 61 (8) (2021) 3891–3898, https://doi.org/10.1021/acs.jcim.1c00203.

[35] O. Trott, A.J. Olson, Autodock vina: improving the speed and accuracy of docking with a new scoring function, efficient optimization, and multithreading, J. Comput. Chem. 31 (2) (2010) 455–461, https://doi.org/10.1002/jcc.21334.

[36] J.G. Motwani, A.D. Struthers, H. Mcalpine, N. Kennedy, Plasma brain natriuretic peptide as an indicator for angiotensin-converting-enzyme inhibition after myocardial infarction, Lancet 341 (8853) (1993) 1109–1113, https://doi.org/10.1016/0140-6736(93)93126-L.

[37] N. Hama, H. Itoh, G. Shirakami, O. Nakagawa, S.I. Suga, Y. Ogawa, I. Masuda, K. Nakanishi, T. Yoshimasa, Y. Hashimoto, M. Yamaguchi, R. Hori, H. Yasue, K. Nakao, Rapid ventricular induction of brain natriuretic peptide gene expression in experimental acute myocardial infarction, Circulation 92 (6) (1995) 1558–1564, https://doi.org/10.1161/01.cir.92.6.1558.

[38] M.A. Matter, F. Paneni, P. Libby, S. Frantz, B.E. Stähli, C. Templin, A. Mengozzi, Y. Wang, T.M. Kündig, L. Räber, F. Ruschitzka, C.M. Matter, Inflammation in acute myocardial infarction: the good, the bad and the ugly, Eur. Heart J. 45 (2) (2024) 89–103, https://doi.org/10.1093/eurheartj/ehad486.

[39] J. Feng, J. Zhan, S. Ma, LRG1 promotes hypoxia-induced cardiomyocyte apoptosis and autophagy by regulating hypoxia-inducible factor-1α, Bioengineered 12 (1) (2021) 8897–8907, https://doi.org/10.1080/21655979.2021.1988368.

[40] A. Saraste, K. Pulkki, M. Kallajoki, K. Henriksen, M. Parvinen, L. Voipio-Pulkki, Apoptosis in human acute myocardial infarction, Circulation 95 (2) (1997) 320–323, https://doi.org/10.1161/01.CIR.95.2.320.

[41] A. Abbate, R. Bussani, G.G. Biondi-Zoccai, R. Rossiello, F. Silvestri, F. Baldi, L.M. Biasucci, A. Baldi, Persistent infarct-related artery occlusion is associated with an increased myocardial apoptosis at postmortem examination in humans late after an acute myocardial infarction, Circulation 106 (9) (2002) 1051–1054, https://doi.org/10.1161/01.cir.0000030936.97158.c4.

[42] M. Viola, S.C.A. de Jager, J.P.G. Sluijter, Targeting inflammation after myocardial infarction: a therapeutic opportunity for extracellular vesicles? Int. J. Mol. Sciences 22 (15) (2021) 7831, https://doi.org/10.3390/ijms22157831.

[43] D. Fraccarollo, P. Galuppo, J. Bauersachs, Novel therapeutic approaches to post-infarction remodelling, Cardiovasc. Res. 94 (2) (2012) 293–303, https://doi.org/10.1093/cvr/cvs109.

[44] R. Zhang, Y. Li, X. Liu, S. Qin, B. Guo, L. Chang, L. Huang, S. Liu, FOXO3a-mediated long non-coding RNA LINC00261 resists cardiomyocyte hypoxia/reoxygenation injury via targeting miR23b-3p/NRF2 axis, J. Cell Mol. Med. 24 (15) (2020) 8368–8378, https://doi.org/10.1111/jcmm.15292.

[45] H. Wang, Q. Feng, Z. Zhang, Y. Gao, R. Li, Clinical efficacy of shexiang tongxin dropping pill combined with conventional therapy in patients with myocardiaischemia reperfusion injury, Journal of Clinical Medicine in Practice 13 (27) (2023) 76–80.

[46] J. Misao, Y. Hayakawa, M. Ohno, S. Kato, T. Fujiwara, H. Fujiwara, Expression of bcl-2 protein, an inhibitor of apoptosis, and BAX, an accelerator of apoptosis, in ventricular myocytes of human hearts with myocardial infarction, Circulation 94 (7) (1996) 1506–1512, https://doi.org/10.1161/01.CIR.94.7.1506.

[47] H. Chen, Y. Chen, X. Wang, J. Yang, C. Huang, Edaravone attenuates myocyte apoptosis through the JAK2/STAT3 pathway in acute myocardial infarction, Free Radic. Res. 54 (5) (2020) 351–359, https://doi.org/10.1080/10715762.2020.1772469.

[48] S. Negoro, K. Kunisada, E. Tone, M. Funamoto, H. Oh, T. Kishimoto, K. Yamauchi-Takihara, Activation of JAK/STAT pathway transduces cytoprotective signal in rat acute myocardial infarction, Cardiovasc. Res. 47 (4) (2000) 797–805, https://doi.org/10.1016/S0008-6363(00)00138-3.

[49] H. Zeng, M. Zhao, Z. Zhang, Z. Liu, S. Zhong, Atorvastatin improves the cardiac function of rats after acute myocardial infarction through ERK1/2 pathway, Eur. Rev. Med. Pharmacol. Sci. 23 (16) (2019) 7120–7127, https://doi.org/10.26355/eurrev_201908_18757.

[50] Y. Lu, M. Yang, M. Peng, L. Xie, A. Shen, S. Lin, B. Huang, J. Chu, J. Peng, Kuanxiong aerosol inhibits apoptosis and attenuates isoproterenol-induced myocardial injury through the mitogen-activated protein kinase pathway, J. Ethnopharmacol. 269 (2021) 113757, https://doi.org/10.1016/j.jep.2020.113757.

[51] J. Zhang, Y. Zhang, S. Xin, M. Wu, Y. Zhang, L. Sun, CXCR7 suppression modulates macrophage phenotype and function to ameliorate post-myocardial infarction injury, Inflamm. Res. 69 (5) (2020) 523–532, https://doi.org/10.1007/s00011-020-01335-z.

[52] X. Liu, S. Ouyang, B. Yu, Y. Liu, K. Huang, J. Gong, S. Zheng, Z. Li, H. Li, H. Jiang, PharmMapper server: a web server for potential drug target identification using pharmacophore mapping approach, Nucleic Acids Res. 38 (suppl_2) (2010) W609–W614, https://doi.org/10.1093/nar/gkq300.

[53] X. Wang, C. Pan, J. Gong, X. Liu, H. Li, Enhancing the enrichment of pharmacophore-based target prediction for the polypharmacological profiles of drugs, J. Chem. Inf. Model. 56 (6) (2016) 1175–1183, https://doi.org/10.1021/acs.jcim.5b00690.

[54] X. Wang, Y. Shen, S. Wang, S. Li, W. Zhang, X. Liu, L. Lai, J. Pei, H. Li, PharmMapper 2017 update: a web server for potential drug target identification with a comprehensive target pharmacophore database, Nucleic Acids Res. 45 (W1) (2017) W356–W360, https://doi.org/10.1093/nar/gkx374.
[55] Q. Yang, D.D. Huang, D.G. Li, B. Chen, L.M. Zhang, C.L. Yuan, H.H. Huang, Tetramethylpyrazine exerts a protective effect against injury from acute myocardial ischemia by regulating the PI3K/AKT/GSK-3β signaling pathway, Cell. Mol. Biol. Lett. 24 (2019) 17, https://doi.org/10.1186/s11658-019-0141-5.
[56] S. Wang, X. Su, L. Xu, C. Chang, Y. Yao, S. Komal, X. Cha, M. Zang, X. Ouyang, L. Zhang, S. Han, Glycogen synthase kinase-3β inhibition alleviates activation of the NLRP3 inflammasome in myocardial infarction, J. Mol. Cell. Cardiol. 149 (2020) 82–94, https://doi.org/10.1016/j.yjmcc.2020.09.009.
[57] D. Zhu, S. Liu, K. Huang, Z. Wang, S. Hu, J. Li, Z. Li, K. Cheng, Intrapericardial exosome therapy dampens cardiac injury via activating foxo3, Circ. Res. 131 (10) (2022) e135–e150, https://doi.org/10.1161/CIRCRESAHA.122.321384.
[58] B.F. Zhang, H. Jiang, J. Chen, X. Guo, Q. Hu, S. Yang, KDM3A inhibition attenuates high concentration insulin-induced vascular smooth muscle cell injury by suppressing MAPK/NF-κb pathways, Int. J. Mol. Med. 41 (3) (2018) 1265–1274, https://doi.org/10.3892/ijmm.2017.3351.
[59] W. Yu, S. Sun, H. Xu, C. Li, J. Ren, Y. Zhang, TBC1D15/RAB7-regulated mitochondria-lysosome interaction confers cardioprotection against acute myocardial infarction-induced cardiac injury, Theranostics 10 (24) (2020) 11244–11263, https://doi.org/10.7150/thno.46883.
[60] S. Sun, W. Yu, H. Xu, C. Li, R. Zou, N.N. Wu, L. Wang, J. Ge, J. Ren, Y. Zhang, TBC1D15-DRP1 interaction-mediated mitochondrial homeostasis confers cardioprotection against myocardial ischemia/reperfusion injury, Metab. - Clin. Exp. 134 (2022) 155239, https://doi.org/10.1016/j.metabol.2022.155239.
[61] B. Zhou, A. Caudal, X. Tang, J.D. Chavez, T.S. Mcmillen, A. Keller, O. Villet, M. Zhao, Y. Liu, J. Ritterhoff, P. Wang, J.S.C. Kolwicz, W. Wang, J.E. Bruce, R. Tian, Upregulation of mitochondrial ATPase inhibitory factor 1 (ATPIF1) mediates increased glycolysis in mouse hearts, J. Clin. Invest. 132 (10) (2022) e155333, https://doi.org/10.1172/JCI155333.
[62] B. Raftrey, I. Williams, P.E. Rios Coronado, X. Fan, A.H. Chang, M. Zhao, R. Roth, E. Trimm, R. Racelis, G. D'Amato, R. Phansalkar, A. Nguyen, T. Chai, K. M. Gonzalez, Y. Zhang, L.T. Ang, K.M. Loh, D. Bernstein, K. Red-Horse, Dach1 extends artery networks and protects against cardiac injury, Circ. Res. 129 (7) (2021) 702–716, https://doi.org/10.1161/CIRCRESAHA.120.318271.